Chapter 4

Heterogeneous Combustion

Jiann C. Yang
National Institute of Standards & Technology
Gaithersburg, Maryland

Introduction

The term "heterogeneous" in this chapter is used loosely to refer to systems in which there are two phases. Under this classification, the subject of heterogeneous combustion is so broad that it is impossible to cover every aspect of it in this chapter. Therefore, only a limited selection of topics will be discussed: liquid droplet combustion, spray combustion, combustion of coal and coal-slurry particle, and smoldering combustion. As a reflection of the author's interest, emphasis will be on liquid droplet combustion and combustion of coal and coal-slurry particles. Discussions on other topics of heterogeneous combustion (e.g., combustion of metal particles, fixed-bed combustion, and fluidized-bed combustion) will not be included because of the voluminous amount of materials to be covered in this chapter.

The importance of droplet combustion stems from the fact that a significant portion of our fuels is consumed in liquid spray combustors. A clear understanding of droplet combustion is an important prerequisite to the understanding of spray combustion.

Spray combustion finds its many usages, to name a few, in gas turbine combustors, diesel engines, industrial furnaces, liquid rocket engines, ramjets, and home oil heaters.

Environmental Implications of Combustion Processes. Chapter 4, CRC Press, Boca Raton, FL, Puri, I. K., Editor(s), 97-137 p., 1993.

The importance of burning of coal particles is self-evident in that many power plants utilize coal as the primary fuel. Moreover, the diminishing petroleum supply has spawned renewed interest in coal utilization because of the vast coal reserves. However, direct utilization of coal is less attractive in that difficulties in transportation, handling, and storage often arise. In addition, coal may not be directly used in many existing liquid-fueled combustors without significant amount of combustor modifications. One way to alleviate such problems is to mix finely crushed coal with oil or water to form a coal/oil (COM) or coal/water (CWM or CWS) slurry mixture. The resulting mixture has certain advantages over coal. It can be transported in existing pipelines for oil, eliminates the danger of spontaneous combustion that often occurs in stored coal, and can be used as an alternate liquid fuel in conventional liquid-fueled combustors. Furthermore, COM is an effective means of reducing oil consumption and is cheaper than oil in many countries or localities where coal is abundant and oil is in short supply. Although CWS has a heating value less than COM, the use of CWS is more appealing than COM because of the complete replacement of the use of oil. Despite the advantages just described, many problems still exist in using CWS and COM. Some of the major concerns are erosion, corrosion, and plugging of components (e.g., atomizers) in the combustor, stability of the mixture during long-term storage, rheological properties of the mixture, and long-term operational reliability.

Smoldering is another mode of heterogeneous combustion, and due to its importance in fire safety it will be briefly introduced at the end of the chapter.

4.1 Fundamentals of droplet and spray combustion

4.1.1 Mechanisms of liquid droplet combustion

A phenomenological description of a burning droplet is first considered. If a liquid fuel droplet is burning in a stagnant, gravity-free (no buoyancy), and oxidizing environment of infinite extent, a spherically-symmetric flame will be formed around the droplet at some distance from the droplet surface, as illustrated in Fig. 4.1. Oxidant and fuel vapor diffuse radially inwards and outwards respectively. At the flame front, oxidant and fuel vapor react stoichiometrically, infinitely fast and intensely, thus forming an infinitely thin flame sheet. Hence, the concentrations of oxidant and fuel vapor are assumed to be zero at the flame zone. No oxidant and fuel vapor can leak through the flame sheet, that is, no oxidant is found on the fuel side of the flame and no fuel vapor, on

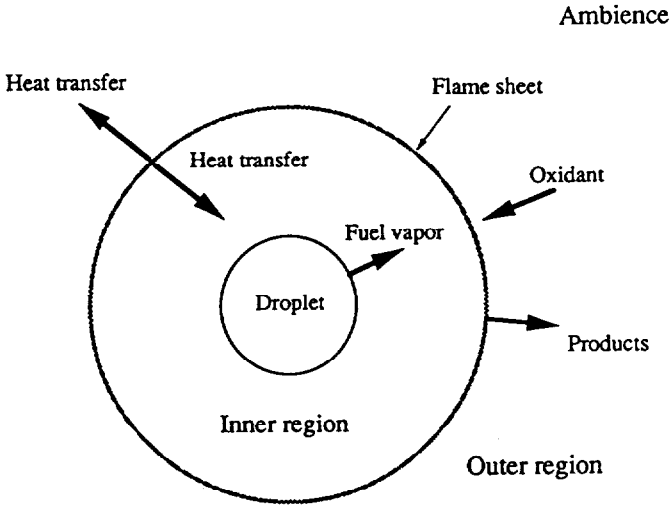

Figure 4.1: Schematic diagram of a fuel droplet burning in an oxidant ambient that is quiescent.

the oxidant side. The heat generated at the flame due to chemical reactions is transported radially outwards to the ambience and inwards to the droplet surface for sustaining evaporization of fuel from the droplet surface.

The classical droplet combustion model, the so–called d^2–Law, was developed in the nineteen fifties by Godsave [215] and Spalding [216]. The model has been used to predict droplet burning rates and to determine droplet burning times in combustors. Such information is essential to the design of spray combustors. Although the model is simple, it provides most of the essential physics of burning of a droplet. The derivation of the d^2–Law will be presented in this section. Although there exist several methods to derive the d^2–Law, the procedure given by Law [217] is adopted here.

Major assumptions that are used in the derivation of the d^2–Law are now discussed. Some of these have already been implicitly mentioned in the discussion pertaining to the phenomenological description of the model.

1. Spherical symmetry. This assumption implies that the droplet is not subject to forced and natural convection. That is, the Reynolds number $Re(= Dv/\nu) \approx 0$, and the Grashof number $Gr(= g\beta\Delta T D^3/\nu^2) \ll 1$ where D, v, ν, g, β, and ΔT are the droplet diameter, velocity, kinematic viscosity, gravitational accel-

eration. thermal expansion coefficient. and temperature difference between flame and ambient respectively. The consequence of this assumption is that non-radial motion in the gas-phase is absent. Hence. the analysis reduces to one dimension, i.e.. all the gas-phase variables (e.g., temperature, species concentrations etc.) are functions of the radial direction only.

The dimensionless Grashof number deserves some attention. From its definition. several ways to minimize natural convection (i.e.. $Gr \ll 1$) are revealed. namely, (a) reducing the ambient pressure. (b) increasing the ambient temperature, (c) reducing the droplet diameter. and (d) reducing the gravitational force.

2. Gas-phase quasi-steadiness. Because gas densities are much smaller than the liquid densities under sub-critical conditions. the characteristic time for changes in the gas-phase is usually much shorter than the droplet surface regression rate. However. the quasi-steady assumption breaks down at, or near. super-critical conditions.

3. Absence of droplet-droplet interaction. Only an isolated droplet in an infinite oxidant ambient is considered. There are no neighboring burning droplets. This assumption may not be valid in a dense spray.

4. Constant gas-phase physical properties.

5. The "flame-sheet" approximation [1] is invoked.

6. Constant and uniform droplet temperature.

7. No internal liquid motion inside the droplet.

8. Single component fuel.

9. No Soret or Dufour effects.

10. No radiative transfer between the flame and droplet surface.

With the above assumptions. and recognizing that the diffusive. convective. and reactive processes occur *only* in the gas-phase. the governing equations in the gas-phase are

$$\nabla \cdot (\rho \vec{v}) = 0 \qquad \text{(continuity).} \tag{4.1}$$

$$\nabla \cdot (\rho \vec{v} Y_i - \rho D \nabla Y_i) = R_i \quad i = F.O \quad \text{(species).} \tag{4.2}$$

$$\nabla \cdot (\rho \vec{v} C_p T - \lambda \nabla T) = q \qquad \text{(energy).} \tag{4.3}$$

where ρ, $\vec{v}$. Y_i. D. R_i, C_p. T, λ, and q are the density. velocity vector, mass fraction of species i, diffusivity. volumetric chemical production/destruction of species i. specific heat, temperature. thermal conductivity, and the volumetric chemical heat generation rate. respectively.

In Eqs. 4.2 and 4.3, the first and second terms represent convective and diffusive transport respectively, while the third term is the chemical source/sink term.

The formation of products from the reaction between a fuel F and an oxidizer O is a complicated process that involves a sequence of intermediate reactions, and a host of intermediate species (cf. Chapter 1). Furthermore, except for some simple fuels, the detailed reaction mechanisms for the oxidation of hydrocarbon fuels are usually not well known. Therefore, it is frequently useful to approximate the detailed kinetic scheme as an overall one–step reaction given by

$$F + \sigma_O O \xrightarrow{Q} \text{Products}, \tag{4.4}$$

where σ_O is the stoichiometric oxidizer–to–fuel mass ratio, and Q is the heat of combustion per unit mass of fuel that is reacted.

The consumption rate of F can be expressed as

$$R_F = -k\rho_O^a \rho_F^b, \tag{4.5}$$

where a and b are respectively called the *reaction orders* with respect to the oxidizer and the fuel, and k is the *kinetic rate constant* which can usually be correlated by the Arrhenius equation (cf. Chapter 1) $k = A\exp(-E/RT)$ where A is the *frequency factor* which is a measure of the collision frequency between the reactants, R is the universal gas constant, and E denotes the activation energy.

Since $\rho_i = Y_i\rho$, Eq. 4.5 can be written in the form

$$R_F = -A\rho^{a+b} Y_O^a Y_F^b \exp(-E/RT). \tag{4.6}$$

From stoichiometry and Eq. 4.4, we have $R_O = \sigma_O R_F$, and $q = -QR_F$.

Due to the highly non–linear nature of the reaction rate terms in Eqs. 4.2 and 4.3 and the coupling of species mass fractions and temperature, it is impossible to obtain an analytical solution without considerable simplification. One such simplification is the assumption of unity Lewis number, i.e., $Le = \lambda/(C_p\rho D) = 1$. With $Le = 1$, it is readily seen from Eqs. 4.2 and 4.3 that Y_i and T are governed by the same differential operator. Therefore, it is possible to remove the highly non–linear source terms in these equations by identifying a suitable linear combination of dependent variables in order to express the equations in a common form. Such a combination is generally referred to as a *coupling function*. If we define a coupling function

$$\beta_i = (Y_i/\sigma_i) + (C_pT/Q), \tag{4.7}$$

where $\sigma_F = 1$ (by definition) from Eq. 4.4, a linear combination of Eqs. 4.2 and 4.3 results in

$$-\nabla\cdot(\rho\vec{v}\beta_i - \rho D\nabla\beta_i) = 0, \tag{4.8}$$

which is used to replace Eq. 4.2 as one of the governing equations. The function β_i is a *conserved scalar* since only the convective and diffusive terms appear in the governing equation, the source/sink term having been eliminated. If $\rho\vec{v}$ is known, then Eq. 4.8 is decoupled from Eq. 4.3. One can first solve Eq. 4.8 for β_i, and then substitute $Y_i/\sigma_i = \beta_i - (C_pT/Q)$ into Eq. 4.3 to solve for T. This procedure is also called the *Shvab-Zel'dovich formulation* [1].

From assumptions (1) and (2), only variations in the radial direction are important. The Eqs. 4.1– 4.3 can be written in the form

$$\frac{1}{r^2}\frac{d}{dr}(\rho r^2 v) = 0. \tag{4.9}$$

From Eqs. 4.3 and 4.8,

$$\rho v C_p \frac{dT}{dr} - \frac{\lambda}{r^2}\frac{d}{dr}\left(r^2\frac{dT}{dr}\right) = QA\rho^{a+b}Y_O^a Y_F^b \exp(-E/RT). \tag{4.10}$$

$$\rho v \frac{d\beta_i}{dr} - \frac{rD}{r^2}\frac{d}{dr}\left(r^2\frac{d\beta_i}{dr}\right) = 0, \tag{4.11}$$

subject to the following boundary conditions, i.e.,

$$\begin{aligned} &\text{At } r \to \infty: \\ &Y_O = Y_{O\infty}, \qquad Y_F = 0, \qquad T = T_\infty \end{aligned} \tag{4.12}$$

$$\begin{aligned} &\text{At } r = r_s: \\ &\rho v_s Y_O - \rho D\frac{dY_O}{dr} = 0, \quad \rho v_s Y_F - \rho D\frac{dY_F}{dr} = \rho v_s. \\ &\lambda\frac{dT}{dr} = \rho v_s L, \qquad T = T_s, \end{aligned} \tag{4.13}$$

where L is the latent heat of vaporization. The third of Eqs. 4.13 implies that droplet heating is negligible, i.e., all the heat transferred to the droplet surface is solely used for vaporization of the fuel. The droplet surface temperature, T_s, can be approximated by the boiling point of the liquid fuel. The error introduced by such an approximation has been discussed by Williams [1], and the approximation has been shown to be valid for most hydrocarbon fuels.

From Eq. 4.9,

$$\rho r^2 v = \rho r_s^2 v_s = M = \text{constant}. \tag{4.14}$$

where $m_s = 4\pi M$ is the burning rate of the liquid droplet. The boundary conditions for β_i are readily derived from Eqs. 4.12–4.13.

$$\text{At } r \to \infty:$$

$$\beta_O = (Y_{O\infty}/\sigma_O) + (C_pT_\infty/Q), \qquad \beta_F = (C_pT_\infty/Q), \tag{4.15}$$

At $r = r_s$:

$$\frac{\lambda}{C_p}\frac{d\beta_O}{dr} = \frac{M}{r_s^2}\left(\frac{Y_O}{\sigma_O} + \frac{L}{Q}\right), \quad \frac{\lambda}{C_p}\frac{d\beta_F}{dr} = \frac{M}{r_s^2}\left(\frac{L}{Q} - (1 - Y_F)\right) \tag{4.16}$$

Integrating Eq. 4.11, we obtain

$$-\frac{1}{r} = \frac{\rho D}{M}\ln\left(\frac{(Y_O/\sigma_O)Q + C_p(T - T_s) + L}{(Y_{O\infty}/\sigma_O)Q + C_p(T_\infty - T_s) + L}\right) \text{ . and} \tag{4.17}$$

$$-\frac{1}{r} = \frac{\rho D}{M}\ln\left(\frac{QY_F + C_p(T - T_s) + L - Q}{C_p(T_\infty - Ts) + L - Q}\right). \tag{4.18}$$

Thus, the problem is reduced to the solution of Eq. 4.10 for T with Y_O and Y_F given by Eqs. 4.17 and 4.18. If a flame–sheet approximation [1] is invoked, then

$$\text{At } r = r_s: \quad T = T_f, \text{ and} \quad Y_O = Y_F = 0, \text{ and} \tag{4.19}$$

$$\text{For } r \leq r_f: \quad Y_O = 0. \tag{4.20}$$

the subscript f denoting conditions at the surface of the flame–sheet. Hence, Eq. 4.17 takes the form

$$-\frac{1}{r} = \frac{\rho D}{M}\ln\left(\frac{C_p(T - T_s) + L}{(Y_{O\infty}/\sigma_O)Q + C_p(T_\infty - T_s) + L}\right). \tag{4.21}$$

For positions lying at radii $r \geq r_f$, $Y_F = 0$ so that Eq. 4.18 may be written in the form

$$-\frac{1}{r} = \frac{\rho D}{M}\ln\left(\frac{C_p(T - T_s) + L - Q}{C_p(T_\infty - T_s) + L - Q}\right). \tag{4.22}$$

Applying Eq. 4.19 to the Eqs. 4.17 and 4.18 and eliminating T_f from the two resulting equations, we obtain an expression for the flame radius, namely,

$$r_f = M/(\rho D \ln(1 + Y_{O\infty}/\sigma_O)). \tag{4.23}$$

Evaluating the Eq. 4.21 at $r = r_s$, with $T = T_s$, the burning rate is obtained, i.e.,

$$m_s = 4\pi M = 4\pi\rho D r_s \ln(1 + B), \tag{4.24}$$

where the quantity B is called the *Spalding transfer number*, and is defined by the following expression:

$$B = (C_p(T_\infty - T_s) + (Y_{O\infty}Q/\sigma_O))/L. \tag{4.25}$$

The transfer number B represents the ratio of the driving force for vaporization to the resistance to vaporization.

The flame temperature T_f is obtained by evaluating Eq. 4.17 at $r = r_f$ with $T = T_f$, and substituting Eq. 4.23 into Eq. 4.17. The expression that is obtained is of the form

$$C_p(T_f - T_\infty)/(Y_{O\infty}/\sigma_O) + L + C_p(T_f - T_s) = Q. \tag{4.26}$$

Substituting Eq. 4.24 into Eq. 4.23. the flame-front standoff ratio, (r_f/r_s) is obtained, i.e.,

$$r_f/r_s = \ln(1 + B)/\ln(1 + Y_{O\infty}/\sigma_O). \tag{4.27}$$

If the fuel evaporization rate at the droplet surface is equal to the consumption rate at the flame. then

$$-\frac{d}{dt}\left(\frac{4}{3}\pi r_s^3 r_l\right) = m_s = 4\pi M, \tag{4.28}$$

where r_l is the density of the liquid fuel, the subscript l denoting conditions at the droplet surface. Substituting Eq. 4.24 into Eq. 4.28 and integrating Eq. 4.27 yields

$$d_s^2 = d_{so}^2 - Kt. \tag{4.29}$$

The quantity K is known as the evaporation or burning rate constant, and is defined as

$$K = (8\rho D/r_l)\ln(1 + B). \tag{4.30}$$

Equation 4.29 is generally referred to as the d^2–Law, which states that the square of the droplet diameter decreases linearly with time as combustion progresses. Note that K is independent of droplet diameter and is constant for a given fuel and ambient conditions. The flame-front standoff ratio is also constant. Equation 4.29 can be used to calculate the total burning time t_b of a droplet by setting $d_s = 0$. i.e.,

$$t_b = d_{so}^2/K. \tag{4.31}$$

Equation 4.31 forms the basic rationale for atomization of liquid fuels for combustion. Atomization results in a large number of small droplets, and, therefore, a significant increase of total surface area for evaporation. and in a reduction of total burning time due to smaller droplet diameters. Although the d^2–Law represents an ideal and simplified case of droplet burning, it nevertheless provides a first estimate of droplet burning rate. Relaxation of some of the assumptions introduced above have been reported by various investigators in order to provide explanations for the observed discrepancies between theoretical predictions and experimental observation.

Upon ignition, it is experimentally observed (e.g. [218, 219]) that the droplet diameter remains relatively unchanged for a brief period. This

behavior is due to the fact that the initial burning rate is very low, and most of the heat transferred from the flame to the droplet is used to heat up the initially cold droplet to a temperature high enough to sustain steady burning. Inclusion of droplet heating in the formulation of droplet burning has been studied by Law [220] and Law and Sirignano [221].

Another experimental observation [222]–[232] inconsistent with predictions obtained using the d^2–Law involves the the variation of the flame–front standoff ratio with time; the d^2–Law gives a constant standoff ratio (cf. Eq. 4.27). Law et al. [219] suggest that the observed behavior of the standoff ratio is caused by fuel vapor accumulation in the inner region of the flame, i.e., the vaporization rate of the fuel droplet is not equal to the consumption rate of fuel vapor at the flame–sheet. In the derivation of the d^2–Law, all the fuel vapor that leaves the droplet surface is implicitly assumed to be completely consumed at the flame. When fuel accumulation is considered in the formulation, the predicted flame-front standoff ratio is found to agree reasonably with experimental observations [219].

Relaxation of the gas–phase quasi–steadiness assumption has been studied by Waldman [233], Crespo and Linan [234], and Matalon and Law [235]. Perturbation methods have been used to solve the governing equations. the ratio of the ambient gas density to the liquid fuel density being the perturbation parameter. Consideration of variable physical properties in the droplet burning formulation has been carried out by Kassoy and Williams [236], Law and Law [237, 238], Chung and Law [239]. and recently by Puri and Libby [240].

In the discussion above, forced or natural convection effects are not considered. If such effects arise, distortion of spherical flame shapes result. and the burning rates must be modified. Correction factors for burning rates under forced convection have been proposed, and used to correlate experimental data [241]. such as,

$$K_{fc} = K_o(1 + 0.276 Re_\infty^{1/2} Sc_\infty^{1/3}), \tag{4.32}$$

where K_{fc} is the burning rate constant with forced convection. K_o the burning rate obtained from the d^2–Law, i.e., under quiescent conditions, and Re_∞ and Sc_∞ are the Reynolds and Schmidt numbers evaluated at ambient conditions. For natural convection, an empirical correction for the burning rate constant has been proposed [241, 242]. i.e.,

$$K_{nc} = K_o(1 + 0.533 Gr^{0.52}), \tag{4.33}$$

where K_{nc} is the burning rate constant in the presence of natural convection and Gr is the Grashof number evaluated at the average temperature of the flame and the ambient. For combined forced and natural convection correction. the following empirical correlation is suggested [241],

namely,

$$K = K_o(1 + 0.276Re_\infty^{1/2}Sc_\infty^{1/3})(1 + 0.533Gr^{0.52}). \qquad (4.34)$$

Up to this point, the discussion has been based on the fact that the fuel contains a single component. In reality, most commercial fuel blends are "multicomponent". Extensive studies have been conducted to examine the combustion characteristics of multicomponent fuels (e.g., [243]–[261]).

A multicomponent analog of the classical single component d^2–Law has been formulated by Law & Law [249]. The derivation is based on the assumption that due to liquid–phase diffusional resistance, a steady–state concentration boundary layer exists at the droplet surface whereas the liquid concentration distributions in the inner core of the droplet remain relatively unchanged during much of the droplet lifetime. The burning rate constant derived for a multicomponent droplet is

$$\begin{aligned} K &= (8\lambda_g/(C_g(\sum Y_{ilo}/\chi_i)/(\sum Y_{ilo}/\chi_i\rho_{il})) \\ &\quad \times \ln(1 + (C_g(T_\infty - T_s) + (Y_{O\infty}/(\sum Y_{ilo}\nu_i))\sum Y_{ilo}Q_i) \\ &\quad /(\sum Y_{ilo}L_i))). \end{aligned} \qquad (4.35)$$

with $\chi_i = (P_n/P_\infty)\,exp((L_i/R_i)(1/T_{bni} - 1/T_s))$, and $T_s \approx \sum X_{ilo}T_{bi}$, where λ_g is the gas–phase thermal conductivity coefficient. C_g the gas–phase specific heat. Y_{ilo} the initial liquid–phase mass fraction of component i, ρ_{il} the liquid–phase density of component i, T_∞ the ambient temperature, T_s the droplet surface temperature, $Y_{O\infty}$ the ambient oxygen mass fraction, ν_i the stoichiometric oxidizer to fuel mass ratio. Q_i the specific heat of combustion of component i, L_i the specific heat of vaporization of component i. P_n the normal atmospheric pressure. P_∞ the ambient pressure. R_i the gas constant of component i, T_{bni} its normal boiling point, X_{ilo} its initial liquid–phase mole fraction, and T_{bi} its boiling point. The d^2–Law appears to work reasonably well for mixtures with similar component volatilities, and for a binary–mixture droplet [249].

For mixtures with dissimilar component volatilities, three-staged combustion behavior has been experimentally observed [251, 253, 256]. In the first stage, the more volatile component starts to vaporize after initial droplet heating. During this period, the droplet temperature, which is governed by the boiling point of the more volatile component, is still relatively low, and the replenishment of the more volatile component at the droplet surface boundary layer from the inner core of the droplet is hindered by the liquid–phase diffusional resistance, resulting in relatively unchanged concentration profiles in the inner core. As time progresses, the less volatile component becomes increasingly concentrated in a boundary layer near the droplet surface due to the depletion of the

more volatile component, and the droplet surface temperature slowly rises to the boiling point of the less volatile component in order to accommodate its vaporization. Therefore, a short transient droplet heating period to bring up the droplet surface temperature follows after preferential vaporization of the more volatile component. This period is termed the second stage which is subsequently followed by the third stage in which vaporization of both components becomes intensive again. The relative duration of the three stages depends on the initial concentration of the mixture [251].

An interesting and important phenomenon, termed *micro-explosion*, associated with multicomponent droplet combustion is the potential for sudden, and frequently violent, explosion or fragmentation of the burning droplet. Micro-explosion has been experimentally observed [246]-[251], [253, 257]. Its occurrence involves superheating of the volatile liquid component which is trapped within the droplet interior because of the liquid-phase diffusional resistance. A bubble forms by homogeneous nucleation [262]. If the bubble growth rate is fast enough, the droplet explodes due to a high internal pressure build-up. For micro-explosions to occur it is necessary for the droplet temperature at some point to exceed the superheat limit of the mixture, which is a state at which homogeneous nucleation can be initiated, i.e.,

$$T_d(r,t) > T_{sh}(X,P), \tag{4.36}$$

where T_d is the temperature of the droplet at location r and time t, and T_{sh}, a function of all the species mole fractions X and pressure P, is the superheat limit of the mixture. The superheat limit of mixture can be estimated by the generalized corresponding principles [262]. The above criterion has been successfully used to predict the occurrence of micro-explosions [232, 247, 253, 257].

Other aspects of droplet combustion (e.g., high pressure conditions, internal circulation in the droplet, ignition, extinction, etc.) are beyond the scope of this chapter. Interested readers are encouraged to consult the excellent review articles by Faeth [17, 263], Law [15, 217, 252], [264]-[266], Sirignano [16], and Williams [267, 268].

4.1.2 Characterization of sprays

The term *spray* in general refers to a two-phase system in which a condensed phase, liquid or solid, is dispersed in a gas-phase. The condensed phase is also known as the dispersed phase, while the gas-phase is sometimes referred to as a continuous phase. Spray combustion, in the form discussed in this chapter, involves the burning of liquid droplets in a gas although the formulations, in principle, also apply to the combustion of solid particles (e.g., to pulverized-coal burners). Spray combustion finds

many uses, for instance, in gas turbine combustors, diesel engines, industrial furnace, liquid rocket engines, ramjets, carburetors, and domeestic oil-heaters.

Sprays are formed by a hydrodynamical process, called atomization. Atomization of liquid fuel is most commonly achieved by injecting the liquid through small orifices at high pressure. Although the atomization mechanism is quite complicated, and is dependent on the nature of the orifice being used and the physical properties of the liquid fuel being atomized, the basic mechanism usually involves the formation of thin liquid sheets, or a primary jet, from the orifice. These sheets subsequently become unstable due to a Rayleigh instability and then break up to form ligaments and large droplets, which break up further into smaller droplets. In a dense spray, collisions and agglomerations between droplets also occur during the latter stage.

The spray, thus formed, is mixed with the combustion air prior to injection into the combustion chamber. The mixing process is critical in determining how overall spray combustion proceeds. Depending on the way in which the fuel spray and the combustion air are mixed, two modes of combustion can be identified: (1) heterogeneous and (2) homogeneous. In the "heterogeneous" spray combustion, the droplets burn either individually or as groups with envelope flames around the droplets. The combustion mechanism is heterogeneous in that both liquid and gas-phases are present. In homogeneous spray combustion, the fuel droplets evaporate completely into fuel vapor prior to arriving at the combustion zone.

The qualitative description given above is a simplification. Indeed, spray combustion is a complicated subject. In order to understand the physical processes of spray combustion, one needs to know (1) the drop size distribution, (2) the combustion mechanism of individual droplets, (3) the nature of droplet-droplet interaction, (4) the mixing processes between the spray and the oxidizing gas (e.g., influences of turbulence), (5) gas-phase ignition, (6) chemical reactions in the gas-phase, and (7) extinction. Modeling of spray combustion that includes all of the above considerations is extremely difficult, if not impossible at this time. Hence, simplifications and limitations need to be imposed in order to render any modeling effort manageable.

4.1.3 Modeling of spray combustion

The theoretical modeling of spray combustion is of considerable importance in the design, development, and improvement of a combustor because it circumvents the strenuous testing of prototypes by cut and try methods, saves costs and reduces the time involved in development. The following discussion of modeling of spray combustion is by no means

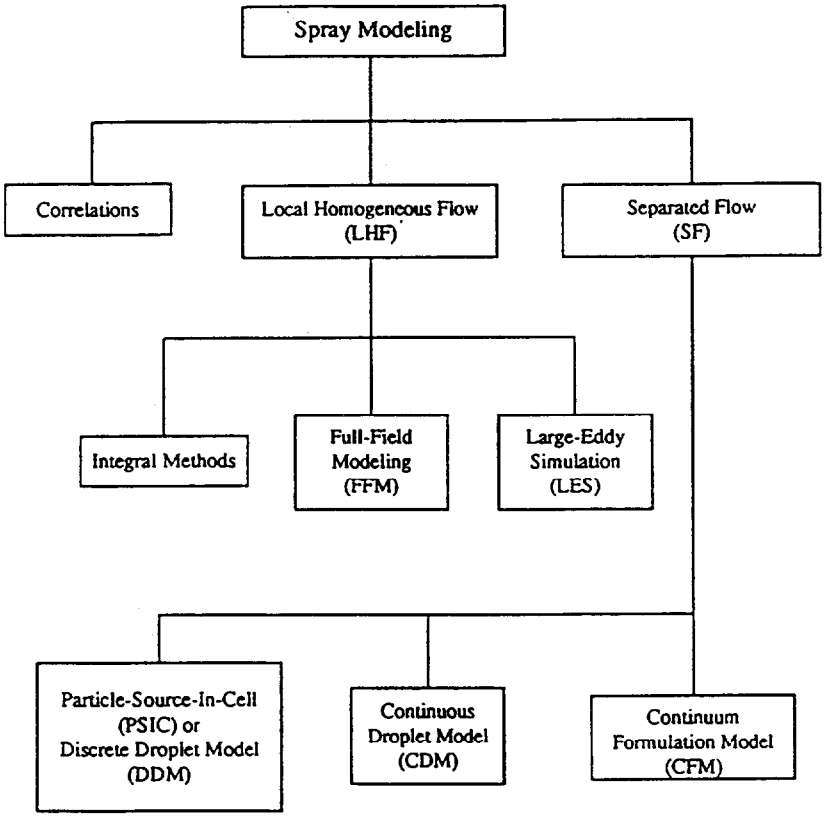

Figure 4.2: Summary of approaches used in spray modeling.

complete. Interested readers should consult the excellent reviews by Faeth [17, 263]. The focus here is to delineate the usefulness and limitation of different models. Fig. 4.2 summarizes the various approaches used in spray modeling.

Correlations

This is probably the simplest approach to attempt to understand spray combustion. Empirical correlations for certain important parameters are obtained by performing experiments. One limitation to this approach is that the correlations are only good for the specific spray combustor and experimental conditions used in the study from which they are obtained.

Locally homogeneous flow (LHF) models

The next level of sophistication in spray modeling is to treat or approximate a spray as a single–phase flow system, since it has long been recognized that spray flames have the flame structure and appearance similar to that of a gas jet–flame. The basic assumption on which LHF models are based is that the rate of development of the flow field is much slower than the interphase transport rates. This requires that all phases be in dynamic and thermodynamic equilibrium, and have the same velocity and temperature at each point in the flow field. In other words, it is mixing that controls the processes in an LHF model.

The LHF models are good approximations for (1) sprays with infinitesimally small droplets, (2) two-phase flow systems (bubbly flows) in which the dispersed phase is a gas or vapor and the continuous phase is liquid due to the rapid attainment of local velocities and temperatures by the bubbles, and (3) sprays at supercritical conditions where the characteristics of both phases are similar.

Since initial drop size and velocity distributions are essentially not required in LHF modeling, one of the advantages of using LHF models to study sprays is that little information concerning the injector properties (which are very difficult to characterize) is required to carry out the computations. A second advantage of using LHF models is that the computation is not as complex and time consuming as SF models, and existing computer codes for single–phase flow calculations can be used with few modifications required in LHF models. A third advantage is that far fewer empirical constants are needed in LHF models than in SF models.

There are basically three approaches used in LHF modeling: (1) integral methods, (2) full-field modeling (FFM), and (3) large-eddy simulation (LES). The latter two methods are primarily used in modeling of turbulence flow field.

In the integral method (e.g. Ref. [269]), the governing equations are integrated in a way similar to that used in the boundary layer analysis. One merit of this method is its relatively mathematical simplicity. Under simple and well–defined flow conditions, this integral approach can satisfactorily predict spray flame properties, such as flame length, spray boundaries, and mean velocities and temperatures.

In full-field turbulence modeling (e.g. Ref. [270]), the governing partial differential equations for the flow properties (e.g., velocities, temperature, mixture fraction, etc.) are written in time (Reynolds) averaged or mass-weighted (Favre) averaged forms (cf. Chapter 7). Due to the averaging processes, additional terms representing turbulence effects appear in the resulting set of equations, which are not closed (i.e., there are more unkowns than equations). These terms must be evaluated by

constructing or using a suitable turbulence model so that the number of unknowns becomes the same as the number of equations. The turbulence model that is most widely used due to its computational simplicity and extensive validation is the two-equation (k–ϵ) model in which the equations for turbulent kinetic energy, and its dissipation rate are solved.

Since there are many turbulence scales associated with turbulence flow, the contributions from all the scales have to be taken into account in order to model turbulence flow accurately, and with a sense of generality. Although small scales involved in turbulence phenomena can be characterized more reliably due to their isotropy, modeling of the large scales is difficult due to their anisotropy. One way of removing the uncertainties involved in modeling the large scales in the calculation is to use the LES approach.

LES is a numerical method that involves the calculation of the transient three–dimensional structure of the turbulent flow [271]. In this method, only the turbulence scales that are smaller than the computational grid size are needed in the calculation. As pointed out in the preceeding paragraph, small turbulence scales are well characterized.

Although LES appears to be attractive due to the absence of the not–well characterized large turbulence scales in the calculation, this method is not used routinely as a practical design tool due to substantial computation times required for practical problems.

In summary, although LHF models are approximate in nature, they provide a reasonable first estimation of the performance of a spray process, and indications of improving the atomization process, prior to actual testing.

Separated flow (SF) models

In SF models, transport processes in the liquid and gas–phases and the inter-phase mass, momentum and energy transport are all taken into account. These phenomena are generally needed for satisfactory prediction of practical spray performance. The common practice is to model the inter-phase transfer independently by using empirical expressions for drop drag, and heat and mass transfer, since detailed modeling of the flow field around individual droplets requires substantial computation time. There are generally three different approaches in SF modeling: (1) particle–source–in–cell (PSIC) or discrete droplet model (DDM), (2) continuous droplet model (CDM), and (3) continuum formulation model (CFM).

The basic concept behind the PSIC approach is to treat the condensed (droplet) phase as source terms of mass, momentum, and energy to the gaseous phase equations [272]. The method involves dividing the flow field into a series of cells, and dividing the spray into representa-

tive groups of discrete droplets. These cells may be regarded as control volumes through which droplets traverse. Governing equations in finite-difference forms are then written for the gas-phase with the appropriate source terms representing the effect of droplets on the gas-phase. An Eulerian approach is used to solved the governing equations of the gas-phase. The entire flow field solution is obtained by solving the equations in each cell.

A Lagrangian approach is used to track the droplets through the flow field. The droplet life history is obtained by integrating the equations of motion for the droplets in the flow field and using empirical expressions for the droplet-gas heat and mass transfer. The usefulness of PSIC or DDM models is limited to dilute sprays where no drop-drop interaction is present.

In the CDM approach, a statistical description of the spray is used because of the stochastic nature of the spray process in that conditions are not well defined as to specify the exact size, position, or velocity of each droplet. The droplets in a spray are characterized by a statistical distribution function $f_j(r, \mathbf{x}, \mathbf{v}, t)$, where $f_j(r, \mathbf{x}, \mathbf{v}, t)drd\mathbf{x}d\mathbf{v}$ is the probable number of drops of chemical composition j with radii in the range of dr about r, located in the volume $d\mathbf{x}$ about $\mathbf{x}$ with velocities in the range $d\mathbf{v}$ about $\mathbf{v}$ at time t. An equation describing the time rate of change of f_j can be derived phenomenologically by using procedures similar to that used in the molecular derivation of the conservation equations, as follows:

$$\frac{\partial f_j}{\partial t} = -\frac{\partial}{\partial r}(R_j f_j) - \nabla_{\mathbf{x}} \cdot (\mathbf{v} f_j) - \nabla_{\mathbf{v}}(\mathbf{F}_j f_j) + Q_j + \Gamma_j. \qquad (4.37)$$

for $j = 1, \ldots, M$, where M is the total number of different kinds of droplets classified based on the chemical composition, $R_j = (dr/dt)_j$ is the rate of change of the size r of a droplet of kind j at $(r, \mathbf{x}, \mathbf{v}, t)$. $\mathbf{F}_j = (d\mathbf{v}/dt)_j$ denotes the force per unit mass on a droplet of kind j at $(r, \mathbf{x}, \mathbf{v}, t)$, Q_j is the rate of increase of f_j due to droplet breakup and nucleation, and Γ_j is the rate of change of f_j due to collisions with other droplets. The subscripts, $\mathbf{x}$ and $\mathbf{v}$, on the gradient operators represent derivatives with respect to spatial and velocity coordinates (or spaces) respectively. A detailed derivation of the equation can be found in Williams [1]. Eq. 4.37 is also referred to as the *spray equation.*

Integration of Eq. 4.37, together with the governing transport equations for the gas-phase, will provide the solution for spray properties. The effect of the spray on the gas phase flow field is considered through source terms, representing momentum, heat, and mass exchange processes between the droplets and the gas-phase, included in the conservation equations of the gas phase.

One limitation that prevents the CDM method from gaining popularity with respect to other spray modeling approaches is due to the

computer storage problem that arise due to the multi-dimensional space required to specify f_j. This problem is further aggravated when additional variables (e.g., droplet temperature, composition variations) are needed to specify f_j. Another limitation associated with this approach relates to the solution of the final forms of the governing equations which have an integro-differential character.

In CFM modeling (e.g. Ref. [273]), the liquid phase is assumed to be a continuum. The resulting equations describe the gas and liquid phases as if they were interpenetrating continua. However, the validity of the continuum assumption for the liquid phase may be questionable under different flow conditions. Difficulties also arise in modeling the droplet heat-up, the turbulent stress tensor for the liquid-phase, and the turbulent dispersion of droplets. Computer time and storage requirements further penalize the use of CFM approach used to model sprays when multiple liquid-phases must be considered based on the ranges of droplet sizes.

4.2 Pollutant formation during droplet and spray combustion

Theoretical studies of nitric oxide (NO) formation in spherically symmetry single droplet combustion have been carried out by Kesten [274], Altenkirch et al. [275], and Bracco [276]. For a given ambient temperature and pressure, and initial droplet size, the ratio of mass of NO formed to mass of fuel (ethanol) burned is found to initially decrease with time as combustion progresses, and subsequently reaches a steady-state value, which is termed the droplet emission index. For a given ambient temperature and pressure, the emission index of an ethanol droplet was found to increase with initial droplet diameter, whereas for a given ambient pressure and initial droplet diameter, the emission index was found to increase with ambient temperature [274]. Increasing ambient pressure has been determined to increase the droplet emission index.

The NO concentration in the exhaust of a diesel engine was found to increase with increasing fuel/air ratio, until a maximum value was reached [275]. Model prediction, however, indicated continuous increase of NO concentration with the fuel/air ratio. It was suggested that droplet burning was important for low fuel/air ratio, and that at high fuel/air ratios, the fuel might no longer be burning in the form of individual droplets due to a change in the atomization characteristics of the injector , or due to the presence of a fuel rich condition.

In his theoretical study of NO formation in ethanol droplet flames, Bracco [276] concluded that diffusion flames around hydrocarbon droplets burning in air could be a significant source of NO, particularly at high air

temperatures, that a given fuel mass would generate less NO if burned in a fine spray than in a coarse spray, and that even at relatively low air temperatures, fuel-bound nitrogen could significantly enhance NO formation within diffusion flames.

The formation of NO, NO_x, and HCN in the forward stagnation region of a diffusion (heptane and ethanol) flame formed by a porous cylinder was studied by Hart et al. [277] in order to simulate droplet combustion. It was found that the maximum yields of NO and NO_x were located towards the lean side of the maximum temperature, that considerable NO was formed near the liquid surface, and that when the fuel was doped with pyridine, enhancement of NO concentration was found, whereas the amount of HCN formed remained unchanged. It was also found that complete conversion of the nitrogen compound to NO was observed in the spray combustion of gas oil doped with small amount of pyridine and quinoline.

Soot formation by combustion of a hydrocarbon droplet in a high pressure stagnant environment (from 0.1 to 3 MPa) has been studied by Kadota et al. [195]. Their results showed that the mass of soot formed and the sizes of the soot particles increased with pressure. More soot was formed when a droplet was burnt in an oxygen–nitrogen mixture ambience than in a carbon dioxide–oxygen mixture. When the amount of soot formed was plotted against the oxygen concentration in the ambience, a threshold oxygen concentration below which no soot was formed and an oxygen concentration at which maximum amount of soot was obtained were found. For normal paraffins, combustion of heavier hydrocarbon droplets generated more soot than lighter ones.

Soot formation was found to decrease with increasing air velocity when a droplet was burnt in a forced–convective air flow [278]. When the blowing velocity is low, an envolope flame surrounding the droplet is formed. As the air velocity increases above a critical value, called the extinction velocity, the envelope flame can no longer be sustained, and a transition to a much shorter flame, the so–called wake flame, established downstream of the droplet occurs. The envelope flame was found to generate much more soot than the wake flame. At room temperature, the amount of soot formed remained relatively constant over the range of air velocities in the envelope flame regime. An abrupt decrease in the amount of soot formed was observed at the extinction velocity. In the wake flame regime, the amount of soot formed decreased with increasing air velocities until a velocity had been reached above which no amount of soot was measured. However, at high ambient temperature, a maximum soot yield was observed at an air velocity in the envelope flame regime, and the extinction velocity was found to increase with increasing ambient air temperature.

When a droplet was burnt solely under natural convection, the soot

yield increased gradually at first, reached a maximum, and then abruptly decreased with increasing ambient air temperature [278]. Increasing temperature was also found to cause the size of the soot particle to increase, and soot yield increased with increasing initial droplet diameter.

Soot concentration profile in a droplet flame was measured by laser light scattering technique [279]. It was observed that the heavily sooting region was located between the droplet surface and the flame. Adding a moderately sooting fuel to a highly sooting fuel caused the heavily sooting region to shift slightly toward the droplet surface and had an effect on reducing soot in the flame.

Soot emission was controlled by the dynamic characteristics of the droplet flame [280]. The instantaneous amount of soot was found to follow the same trend as the instantaneous change of the flame size. Soot emission was reduced when the flame was small and closed. As long as the soot forming region was confined within the inwardly regressing and closed flame during the course of combustion, near-complete oxidation of soot could result, leading to very little soot emission. Weak convection facilitated soot oxidation while early extinction of the flame led to considerable amount of soot emission. Therefore, it can be concluded that convective flow reduces the residence time of soot precursors in the flame and carries soot precursors to the flame zone where they can be readily oxidized.

The above studies [278, 280] suggest that during combustion a critical instantaneous droplet diameter below which no soot emission occurs exists. This diameter which is termed the sooting limit of a liquid fuel droplet can be used to determine the relative sooting tendencies among liquid fuels [281]. When a droplet was burnt in a convective air flow, it was observed [281] that the sooting limit diameter increased with the air velocity. This indicates that soot emission decreases with increasing air velocity, which is consistent with the experimental observations in Ref. [278].

When a droplet was burnt at low gravity, a condition where spherically symmetric combustion could be realized, observations of a soot shell have been reported in Refs. [227], [229]–[232], [260, 261]. In a spherically symmetric flame, fuel vapor, soot precursors and particles have longer residence times within the flame due to the absence of natural and forced convective flows. Increased residence time may result in increased fuel pyrolysis, increased generation of soot precursors, and more agglomeration of soot particles inside the flame. Once the soot particles are formed, they will be transported inwardly toward the droplet surface by thermopheresis. At the same time, the soot particles are also subjected to the drag force created by the radially and outwardly directed Stefan flow associated with droplet vaporization. The soot particles are thus expected to form a shell-like structure between the flame and the droplet surface,

the location of which is determined by the balance between the Stefan flow and the thermophoretic force.

The existence of a soot shell can affect droplet burning rates in a number of ways [261]. The soot shell may : (1) act as a thermal shield for conduction and radiation from the flame to the droplet surface, (2) act as a diffusion barrier by reducing the mass flux of fuel vapor to the flame, and (3) provide reaction sites for diffusing fuel molecules. Lower burning rates would therefore result from the reduction in heat transfer to the droplet and mass transfer of fuel vapor to the flame due to the presence of the shell.

The effect of initial droplet diameter on soot formation and burning rate can now be addressed based on the residence time of fuel molecules in the flame. The residence time was found to be approximately proportional to the droplet size squared [261]. Thus, larger droplets have longer residence times which could allow for more soot precursors to form and subsequent generation of more soot particles. The increase in soot formation for larger droplets could lead to the formation of thicker soot shells which could correspondingly reduce the heat and mass transfer rates between the droplet and the flame and hence the burning rates.

Formation of a soot shell would sometimes lead to the disruptive burning of the droplet [227, 231]. It was suggested that such disruption might be the result of the dissolution of the gas phase pyrolysis products into the liquid phase [282]. The absorption of species from the gas phase would render the initially pure liquid droplet multicomponent, and the subsequent disruptive burning of the droplet would therefore resemble the micro-explosion phenemenon observed during the combustion of a multicomponent droplet.

From the above description of soot formation in droplets, it appears that mixing and atomization would play two important roles in soot formation in spray flames. The degree of mixing in the spray flame controls the local conditions for soot formation. For example, the presence of fuel-rich pockets, as a result of poor mixing, within the spray could lead to significant soot formation by promoting fuel pyrolysis by increasing residence time of fuel molecules. Efficient or improved atomization results in a decrease in droplet size which would in principle lead to less soot formation. However, a reduction in droplet size would decrease spray penetration into the combustor due to the reduced momentum associated with smaller droplets. When coupled with inadequate mixing, a fuel-rich region which may facilitate soot formation is formed.

In spray flames, increasing pressure promotes soot formation [283], which is in agreement with the observations from droplet combustion [195].

4.3 Fundamentals of coal particle combustion

4.3.1 Characteristics of coal

Coal is an inhomogeneous organic fuel, formed from large plant masses *via* a sequence of geological processes that have occurred over an extended period of time, often subjected to moisture, high temperatures, and elevated pressures. Depending on the origins of the vegetable matters and the extent of their decay, the composition of coal varies greatly. Typical compositions (mass percentages) of different coals obtained by elemental analysis include 65-95% carbon, 2–7% hydrogen, up to 25% oxygen, up to 10% sulfur, and 1–2% nitrogen [284]. Inorganic mineral matter (ash) as high as 50% has been reported in some instances, but 5–15% is more typical [285]. Moisture content varies from 2–20%, but values as high as 70% has been recorded for some coals. Ash consists primarily of silicon although some coals contain ash which is high in alkaline metals such as calcium, sodium, and magnesium [286]. In addition to mineral matter, about 20 trace elements can be found in coal. Table 4.1 (adopted from Ref. [287]) gives the orders of magnitudes of average trace–element concentrations and the main forms in which some of the trace elements appear in coal.

The composition of coal is generally characterized by ASTM (American Society of Testing and Materials) Ultimate Analysis or ASTM Proximate Analysis. In Ultimate Analysis, the elemental (C, H, N, S, and O, the latter being determined by difference) composition based on a dry basis is provided while the residual mineral matters being shown as ash. Proximate Analysis determines the moisture content by drying, volatile matters by monitoring mass loss from devolatilization at about 1200K in an inert environment, ash classified as residue after oxidation in air, and fixed carbon by difference. Table 4.2 (adopted from Ref. [286]) shows both analyses of a number of U.S. coals.

Depending on the geological age, coals are classified by their *ranks*: older coal is loosely classified as having a higher rank. In general, coals of increasing rank have increasing heating values, higher fixed-carbon level, higher sulfur content, and lower oxygen content [286].

4.4 Combustion mechanisms of coal particles

When a coal particle is subjected to intense heating in an oxidizing environment, the volatile components first evolve from the particle, and then subsequently burn in the gas phase. The evolution of volatiles from the

Table 4.1: Trace elements in coal.

Element	Average Concentration (order of magnitude, in ppm)	Chemical form
Antimony	1	Sulphide
Arsenic	10	Sulphide
Beryllium	1	Organic
Boron	100	Organic
Cadmium	1	Sulphide
Chlorine	1000	Organic & inorganic
Chromium	10	
Cobalt	10	Organic & inorganic
Copper	10	Sulphide
Fluorine	100	
Lead	10	Sulphide
Manganese	100	Carbonate
Mercury	0.1	Sulphide
Molybdenum	1	Organic & inorganic
Nickel	10	Organic & inorganic
Selenium	1	Sulphide
Thallium	1	
Titanium	1000	Aluminosilicate
Thorium	1	
Tungsten	1	
Uranium	1	
Vanadium	10	Organic
Zinc	100	Sulphide

Table 4.2: Coal compositions.

Ultimate analysis (% dry)	Colorado	Pittsburgh No. 8	Western Kentucky	Montana Powder River	Texas Lignite
C	73.1	77.2	73.0	67.2	60.44
H	5.1	5.2	5.0	4.4	4.61
N	1.16	1.19	1.4	1.1	1.21
S	1.1	2.6	3.1	0.9	1.75
O	9.7	5.9	9.3	14.0	14.38
Ash	9.8	7.9	8.2	11.7	17.61
Proximate analysis (%)					
Volatile matter	38.9	37.0	36.1	30.5	28.68
Fixed carbon	52.6	54.0	51.2	39.0	24.08
Moisture	3.3	1.2	4.8	21.2	35.96
Ash	8.9	7.8	7.8	9.2	11.28

particle occurs through several physical mechanisms [286]. One mechanism involves the formation of bubbles in the interior of the particle, migration of these bubbles to the particle surface, and subsequent bursting of the bubbles at the particle surface. The kind of volatile species and the rate at which they evolve may depend not only on the nature of the coal particle considered, but also on the process of bubble formation and passage through the particle [288]. Some coal particles may also exhibit swelling and melting during devolatilization. Another mechanism involves the cracking of the particle surface during pyrolysis, thus allowing volatile species to escape through the cracks. When this occurs, the particle does not swell appreciably during devolatilization.

Volatile species emanating from the coal particle during devolatilization include CO, CO_2, H_2O, HCN, H_2, nitrogeneous species, hydrocarbon liquids, hydrocarbon gases (such as CH_4, C_2H_6, C_2H_4, C_2H_2, etc.), and tars. If the ambient temperature is high enough, some volatiles react with ambient oxygen, and a diffusion flame is formed, surrounding the coal particle.

Heterogeneous combustion, or oxidation, of the involatile carbonaceous residue (char) follows after the volatile species are driven out from the coal particle. Since devolatilization and char oxidation are both dependent on the kind of coal particles used and the ambient conditions in which these two processes are being carried out, different devolatilization models and char oxidation rate schemes have been proposed. In the following sections devolatilization and char oxidation models are discussed.

Devolatilization models

One way to model devolatilization is to approximate the process simply by a global first-order reaction occurring uniformly throughout the coal particle [289]. The rate of devolatilization is expressed as

$$\frac{dV}{dt} = k(V^* - V) \text{ , with} \tag{4.38}$$

$$k = A\exp(-E/RT_p). \tag{4.39}$$

where V is the mass fraction (in terms of the original coal mass) of volatiles lost at time t, V^* is the value of V at $t \to \infty$, T_p is the temperature of the coal particle, and k, which is represented by an Arrhenius rate expression, is the rate constant. Note that V^* is different from the volatile content obtained by proximate analysis since the latter is not determined at the conditions of interest, but rather at some standard reference conditions. The reader should bear in mind that devolatilization depends on the temperature of the coal particle. However, an empirical correlation can be used to relate V^* to that obtained from proximate analysis (V_p) [288].

$$V^* = Q(1 - V_c)V_p. \tag{4.40}$$

where Q and V_c are empirical constants.

The lack of generality and flexibility of Eq. 4.38, and its inadequacy in describing non-isothermal devolatilization, have prompted other researchers to look for more elaborate ways of correlating experimental data. The use of an nth order rate expression instead of a first-order kinetic expression has been proposed by Wiser et al. [290], i.e.,

$$\frac{dV}{dt} = k'(V^* - V)^n. \tag{4.41}$$

The validity of Eq. 4.41 is still questionable, and lacks generality because no single n value can be used to fit experimental data for the entire devolatilization period: n can vary from $n = 2$ at the early stage of devolatilization to $n = 1$ at the later stage of devolatilization [290]. The value of n also depends on the type of coal, and on the experimental conditions.

In an attempt to correlate their data, Kobayashi et al. [291] proposed a parallel competing reaction scheme involving two reactions, namely,

$$\text{Coal } (C) \begin{cases} \xrightarrow{k_1} \overset{\alpha_1}{\text{Volatile 1}}(V_1) + \overset{(1-\alpha_1)}{\text{Residue 1}}(R_1) \\ \xrightarrow{k_2} \overset{\alpha_2}{\text{Volatile 2}}(V_2) + \overset{(1-\alpha_2)}{\text{Residue 2}}(R_2), \end{cases}$$

where k_1 and k_2 are the first order (with respect to C) kinetic rate constants and α_1 and α_2 are the mass fractions of coal produced as volatiles *via* Reactions 1 and 2.

The rate equations for the above devolatilization model are

$$\frac{dC}{dt} = -(k_1 + k_2)C \text{ , and} \tag{4.42}$$

$$\frac{dV_1}{dt} + \frac{dV_2}{dt} = (\alpha_1 k_1 + \alpha_2 k_2)C. \tag{4.43}$$

The kinetic rate constants, k_1 and k_2, are expressed by

$$k_i = A_i \exp(-E_i/RT_p), \quad i = 1, 2. \tag{4.44}$$

At relatively low devolatilization temperatures, Reaction 1 is assumed to be dominant. At high temperatures, Reaction 2 is assumed to proceed faster than the first one. This model has been found to give a better correlation of data than obtained by the single-reaction model (e.g., Eq. 4.38) at moderate and high temperatures [291]. However, generalization of this model is limited by the dependence of the kinetic parameters (A_1, A_2, E_1, and E_2) and α_1 and α_2 on the specific coal type.

Another conceptual approach to modeling devolatilization is to consider a parallel multiple-reaction scheme, namely,

$$\frac{dVi}{dt} = k_i(Vi^* - Vi). \tag{4.45}$$

with k_i given by Eq. 4.44. Integration of Eq. 4.45 results in

$$V_i^* - V_i = V_i^* \exp(-\int_o^\infty k_i dt). \tag{4.46}$$

Since the parameters (A_i, k_i, and E_i) can not be determined a priori, one way to facilitate the use of Eq. 4.46 is to assume that the k_is are the same (i.e., $k_i = k$) in all the reactions and that all E_i's can be expressed by a continuous distribution function $f(E)$, with $dF/dE = f(E)$ where F represents the fraction of the potential volatile loss V^* which has an activation energy less than E. In this case, V_i^* becomes a differential part of the total V^*, and may be written as

$$dV^* = V^* \ dF = V^* f(E)dE. \tag{4.47}$$

with $\int_o^\infty f(E)dE = 1$. Using Eq. 4.47, integration of Eq. 4.46 over all values of E (i.e., summing the contribution from each reaction) yields the total amount of volatile material yet unreleased, namely,

$$V^* - V = V^* \int_o^\infty \exp\left(-\int_o^t k(E)dt\right) f(E)dE. \tag{4.48}$$

A distribution function $f(E)$ has to be assumed in order to use Eq. 4.48 for correlating experimental devolatilization data. A Gaussian distribution function with mean activation energy E_o and standard deviation σ was used by Anthony et al. [292].

$$f(E) = \frac{1}{\sigma\sqrt{2\pi}} \exp\left(-\frac{(E - E_o)^2}{2\sigma^2}\right). \tag{4.49}$$

With this function Eq. 4.48 can be writen as

$$V^* - V = \frac{V^*}{\sigma\sqrt{2\pi}} \int_o^\infty \exp\left(-\int_o^t k(E)dt\right) \times \exp\left(-\frac{(E-E_o)^2}{2\sigma^2}\right) dE. \tag{4.50}$$

Equation 4.50 is found to provide good correlation of the devolatilization kinetics data [292]. At first glance, Eq. 4.50 seems more complicated than Eq. 4.38. However, only one additional parameter is introduced in Eq. 4.50 (i.e., V^*, E, k in Eq. 4.38 *versus* V^*, E_o, σ, k in Eq. 4.50). As

pointed out by Anthony et al. [292], the replacement of E by E_o and σ, and the associated use of the somewhat more complicated equations eliminates the temperature dependence of V^* and allows comparison of data on a given coal type under different sets of experimental conditions with one set of parameter values (V^*, E_o, σ, k), whereas the parameters (V^*, E, k) in the simple first-order model depend on the prevailing experimental conditions. The dependence of the parameters on the coal type and the need to determine *a priori* the parameters for a specific coal still limits the use of the multiple-reaction model. Other more complex devolatilization models, which involve multi-step series-competition schemes, have been comprehensively reviewed by Anthony and Howard [288].

In the above equations, the temperature of the coal particle, T_p, can be estimated by using a lumped-capacitance (i.e., negligible internal thermal resistance within the particle) heat transfer model if the Biot number ($Bi \equiv hL_c/k_p$) ≤ 0.1 [293], where h is the heat transfer coefficient, L_c is the characteristic length (for a sphere of radius r_p, $L_c = r_p/3$), and k_p is the thermal conductivity of the coal particle. If a spherical shape is assumed for the coal particle, the lumped-capacitance model results in

$$\rho_p C_p \frac{4}{3}\pi r_p^3 \frac{dT_p}{dt} = 4\pi r_p^2 \epsilon_p \sigma (T_\infty^4 - T_p^4) + 4\pi r_p^2 h (T_\infty - T_p). \qquad (4.51)$$

where ρ_p is the density of coal particle C_p is its heat capacity, ϵ_p the particle emissivity, σ the Stefan-Boltzmann constant, and T_∞ the ambient temperature. The heat transfer coefficient, h, can be estimated from empirical correlations [293]. In the case of a stagnant ambient, h can be easily calculated by using $Nu \equiv hr_p/k_g = 1$, where Nu is the Nusselt number and k_g is the thermal conductivity of the gas-phase. In this case, the Biot number becomes $Bi = k_g/3k_p$. The condition $Bi \leq 0.1$ can be satisfied if the coal particle is very small, or if the thermal conductivity of the coal particle is very large.

Char oxidation models

Two common and idealized approaches to modeling of char oxidation are [294]: (1) the progressive-conversion model and (2) the shrinking-core model.

Progressive-conversion model In the progressive-conversion model, the oxidation of char is assumed to occur continuously, homogeneously, and progressively throughout the char particle at all times. This model can further be classified as one without a layer of ash formed surrounding the reacting char particle or one with an ash layer (see Fig. 4.3). When an ash layer is absent, the oxidation rate of the char particle can be estimated as follows.

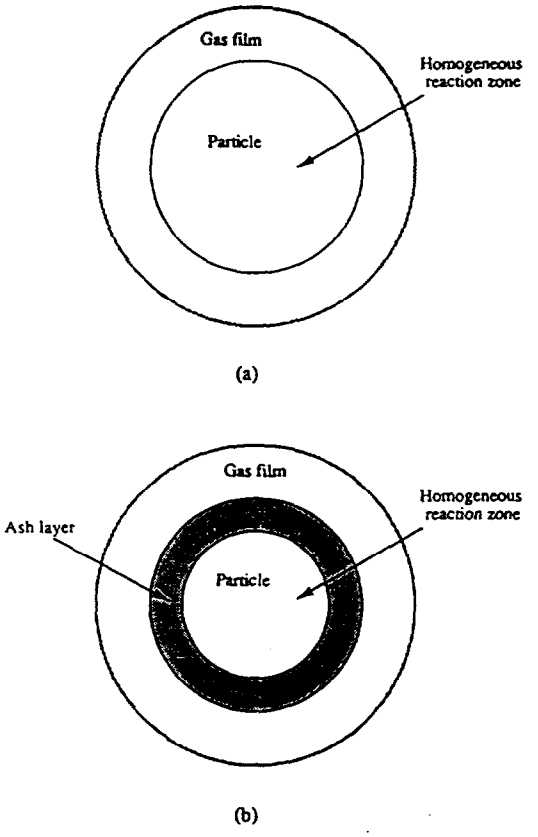

Figure 4.3: Progressive–conversion models: (a) without an ash layer, and (b) with an ash layer.

For simplicity, let us assume the oxidation reaction to be represented by a simple overall first-order reaction:

$$\nu_c[\text{Char}] + \nu_o[\text{O}] \rightarrow \text{ash} + \text{products} \tag{4.52}$$

where ν_c and ν_o are the stoichiometric coefficients of the reaction. Assuming that the char particle is spherical and porous, and that diffusion within the particle can be represented by a constant effective diffusivity D_e, a mass balance on a differential volume of the char particle can be written for the oxidant diffusing through the particle in the radial direction r. Shrinking the differential element to zero gives [13]

$$-D_e \frac{1}{r^2}\frac{d}{dr}(r^2 \frac{dCo}{dr}) = R_o. \tag{4.53}$$

where R_o is the overall *volumetric* reaction rate of the oxidant, $Ro = -k'''C_o$ with k''' being the kinetic rate constant, and C_o is the molar concentration of the oxidant. The boundary conditions are given by

$$\text{At } r = 0, \quad \frac{dC_o}{dr} = 0 \quad \text{or } C_o \text{ is finite.} \tag{4.54}$$

$$\text{At } r = r_c. \quad C = C_{o\infty}\ . \tag{4.55}$$

where r_c is the radius of the char particle and $C_{o\infty}$ is the ambient oxidant concentration. Equation 4.55 is written with the assumption that the diffusional resistance in the gas film surrounding the particle is negligible. Otherwise, Eq. 4.55 becomes

$$\text{At } r = r_c, \ D_e \frac{dC_o}{dr} = k_D(C_{o\infty} - C_o). \tag{4.56}$$

where k_D is the mass transfer coefficient.

A solution to Eq. 4.53 with the boundary conditions implied by Eqs. 4.54 and 4.55, can be obtained by the transformation $f(r) = rC_o$. Thus Eq. 4.53 becomes

$$\frac{d^2 f}{dr^2} - \frac{k'''}{D_e} f = 0. \tag{4.57}$$

The general solution of Eq. 4.57 can be written in terms of C_o as

$$C_o = \frac{C_1}{r}\cosh\left[\sqrt{\frac{k'''}{D_e}}r\right] + \frac{C_2}{r}\sinh\sqrt{\frac{k'''}{D_e}}r]. \tag{4.58}$$

where C_1 and C_2 are integration constants. Application of the two boundary conditions, i.e., Eqs. 4.54 and 4.55, results in the following expression, namely,

$$\frac{C_o}{C_{o\infty}} = \frac{r_c}{r}\frac{\sinh[\sqrt{k'''/D_e}r]}{\sinh[\sqrt{k'''/D_e}r_c]}. \tag{4.59}$$

It is common practice to express the volumetric reaction rate in terms of the reaction occurring at a surface. This is done by the relationship $R_o = aR_o'' = -ak''C_o$ where R_o'' is the reaction rate per unit surface area, a is the surface area per unit volume (of solids and voids) of the char particle, and k'' is the kinetic rate constant which is related to k''' by $k''' = k''a$.

Since the overall rate of oxidant reacted is equal to the total molar flow of the oxidant into the char particle, we obtain

$$W_o = 4\pi r_c^2 D_e \left(\frac{dC_o}{dr}\right)_{r=r_c} \tag{4.60}$$

Substituting Eq. 4.59 into Eq. 4.60 gives

$$W_o = 4\pi r_c D_e C_{o\infty}[\phi \coth \phi - 1] , \tag{4.61}$$

where $\phi = (\sqrt{k''a/D_e})r_c$ is the Thiele modulus, which is a measure of the relative importance of the surface reaction rate to the rate of diffusion within the char particle. When ϕ is large, diffusion is rate–limiting, whereas for small ϕ the surface reaction is the rate–controlling process.

It is often more convenient to express the reaction rate R_o in terms of $C_{o\infty}$ rather than C_o. To accomplish this, one can assume the reaction rate equal to that which would result if the entire internal char surface is exposed to the external surface concentration, $C_{o\infty}$. In this case the molar conversion rate of the oxidant is

$$W_{o\infty} = (4/3)\pi r_c^3 a(k''C_{o\infty}). \tag{4.62}$$

By dividing Eq. 4.61 by Eq. 4.62, an important parameter, the *effectiveness factor* η is defined, where $\eta = (W_o/W_{o\infty}) = (3/\phi^2)[\phi \coth \phi - 1]$. The effectiveness factor is used to correct the reaction rate for internal diffusional resistance.

The *global* reaction rate of the char, W_c, is obtained from the expression $W_c = (\nu_c/\nu_o)W_{o\infty}\eta$. When an ash layer is present, an additional diffusion resistance to the oxidant in the ash layer has to be accounted for.

Since no reactions occur in the ash layer, a mass balance for the oxidant in the ash layer and the reacting char particle results in the expressions

$$\text{Ash layer.} \quad D_e^* \tfrac{1}{r^2}\tfrac{d}{dr}\left(r^2 \tfrac{dC_o}{dr}\right) = 0, \tag{4.63}$$

$$\text{Char particle.} \quad D_e \tfrac{1}{r^2}\tfrac{d}{dr}\left(r^2 \tfrac{dC_o}{dr}\right) = -Ro. \tag{4.64}$$

where D_e^* is the effective diffusivity in the ash layer.

The boundary conditions are

$$r = 0 \quad \frac{dC_o}{dr} = 0, \tag{4.65}$$

$$r = r_c \quad D_e \frac{dC_o}{dr} = D_e^* \frac{dC_o}{dr}, \tag{4.66}$$

$$r = r_a \quad D_e^* \frac{dC_o}{dr} = k_D(C_{o\infty} - C_o). \tag{4.67}$$

Solutions to Eqs. 4.63– 4.67 have been obtained by many investigators by assuming a first–order reaction, an mth order reaction, variable diffusivity, or $D_e = D_e^*$ [295].

Shrinking–core model In a shrinking–core model, the reaction is assumed to occur only at the outer surface of the char particle. As time progresses, the particle shrinks in size due to the radial movement of the reaction front towards the center of the particle. Complete conversion of the char is assumed to occur as the reaction front passes any given point within the char particle. The shrinking–core model can further be classified according to the absence or presence of an ash layer surrounding the shrinking unreacted core (see Fig. 4.4).

Shrinking–core model with no ash layer. In this model, three distinct processes can occur in succession: (1) diffusion of oxidant from the ambient through the gas film to the surface of the char particle, (2) reaction of oxidant with the char on the outer surface of the particle, and (3) diffusion of reaction products from the surface through the gas film back to the ambient.

The last step is normally assumed not to contribute significantly to the rate–determining process unless the diffusion of the reaction products is so slow that a blanket of products are formed in the vicinity of the particle surface, thus providing additional diffusional resistance to the oxidant. To simplified the analysis, it is assumed that gas–film diffusion of reaction products is not important in the present treatment.

Case (1) Rate controlling: gas–film diffusion of oxidant. This limiting condition normally occurs at very high temperatures. Since the gas–film diffusion is the rate–controlling step, an implicit assumption is that the surface reaction between the oxidant and the char is infinitely fast such that the concentration of the oxidant is zero at the particle surface. Additionally, if a quasi–steady assumption is applied to the gas–phase, the oxidant consumption rate is equal to the amount of oxidant transferred through the gas–film to the char surface. Assuming the char particle to be spherical we have $W_o = 4\pi r_c^2 k_D(C_{o\infty} - C_{os})$ where C_{os} is the molar oxidant concentration at the outer char surface.

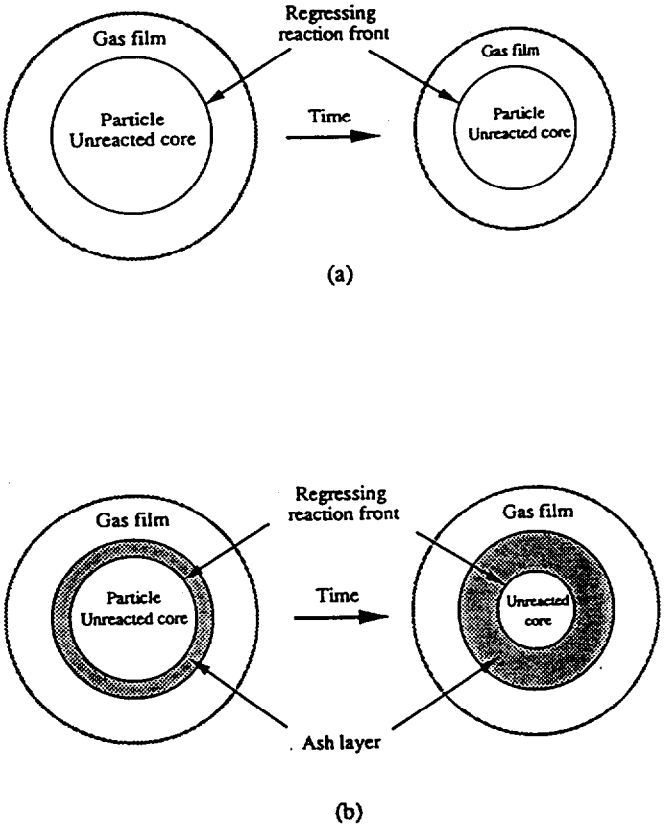

Figure 4.4: Shrinking–core models: (a) without an ash layer, and (b) with an ash layer.

In this case it is equal to zero. From stoichiometry, the rate of char consumption, W_c, is

$$W_c = (\nu_c/\nu_o)W_o = (\nu_c/\nu_o)4\pi r_c^2 k_D C_{o\infty}. \tag{4.68}$$

Since the rate of char consumption is equal to the rate of mass loss of the char, we obtain

$$-\rho_c dV_c/dt = (\nu_c/\nu_o)4\pi r_c^2 k_D C_{o\infty}. \tag{4.69}$$

where ρ_c and $V_c(= (4/3)\pi r_c^3$ are the molar density of the char and the instantaneous volume of the particle respectively.

The mass transfer coefficient can be obtained from Sherwood number (Sh) correlations. For flow past a sphere,

$$Sh \equiv (2r_c k_D/D_o) = 2(1 + cRe^{1/2}Sc^{1/3}), \tag{4.70}$$

where D_o is the oxidant diffusivity. Re is the Reynolds number based on particle diameter, and Sc is the Schmidt number. Typical values for c are $0.30 < c < 0.35$ [295]. If the char particle is very small, or is subjected to a stagnant ambient, then $Re \approx 0$. Under these conditions, $Sh \approx 2$. Hence,

$$k_D = Do/r_c. \tag{4.71}$$

Substituting this expression for k_D into Eq. 4.69, and integrating the resulting equation we obtain

$$d_{co}^2 - d_c^2 = (8D_o C_{o\infty}\nu_c/(r_c\nu_o))t. \tag{4.72}$$

where d_{co} and d_c are respectively the initial and instantaneous diameters of the particle. Thus, we obtain the d^2-Law for char oxidation. The time $(t_b)_{film}$ required for complete oxidation of the char particle can be estimated from Eq. 4.72 by assigning $d_c = 0$. Therefore, $(t_b)_{film} = d_{co}^2 r_c \nu_o/(8D_o C_{o\infty}\nu_c)$.

Case (2) Rate controlling: surface chemical reaction. This rate-limiting condition is characterized by low temperatures and very large char particles. In this case, the gas-film diffusion is assumed to be infinitely fast. Hence, the oxidant concentration at the reacting surface is equal to the ambient oxidant concentration, $C_{o\infty}$. Assuming that the reaction can be represented by

$$\nu_c[\text{Char}] + \nu_o[\text{O}] \rightarrow \text{products}\ . \tag{4.73}$$

and the volumetric oxidation rate, R_o, due to a first-order reaction is

$$R_o = -k'''C_{os}. \tag{4.74}$$

with $C_{os} \approx C_{o\infty}$. Then the rate of oxidant consumption, W_o, is

$$W_o = (4/3)\pi r_c^3(-R_o). \tag{4.75}$$

Since the rate of char consumption is equal to the rate of mass loss of the char particle, the following relation results, i.e.,

$$\begin{aligned} -\rho_c \frac{d}{dt}\left((4/3)\pi r_c^3\right) &= W_c = (\nu_c/\nu_o)W_o \\ &= (\nu_c/\nu_o)(4/3)\pi r_c^3(k'''C_{o\infty}). \end{aligned} \tag{4.76}$$

Upon integration with $k''' = ak''$, where a in this case is simply $3/r_c$, the following equation results, namely,

$$d_{co} - d_c = (2\nu_c/(\nu_o\rho_c))k''C_{o\infty}t. \tag{4.77}$$

and the time $(t_b)_{rxn}$ for complete consumption of the particle is

$$(t_b)_{rxn} = (d_{co}\nu_o\rho_c)\ (2\nu_c k''C_{o\infty}). \tag{4.78}$$

Case (3) Rate controlling: combined effect. In this case, both the gas-film diffusion and the surface chemical reaction have to be taken into account. Assume again that the surface reaction can be represented by a first-order reaction. Since the amount of oxidant transported through the gas film is equal to that reacted at the surface, one can write

$$W_o = (4/3)\pi r_c^3(k'''Cos) = 4\pi r_c^2 k_D(C_{o\infty} - C_{os}). \tag{4.79}$$

Note that the concentration C_{os} cannot normally be measured directly. Substituting $k''' = ak''$ with $a = (3/r_c)$ into Eq. 4.79, the molar concentration of the oxidant at the surface can be expressed in terms of the normally-known concentration $C_{o\infty}$, i.e., $C_{os} = (k_D/(k_D + k''))C_{o\infty}$.

From stoichiometry, and by equating the rate of char consumption to the rate of char mass loss, we obtain

$$\begin{aligned} -\rho_c \frac{d}{dt}\left((4/3)\pi r_c^3\right) &= W_c = (\nu_c/\nu_o)W_o \\ &= (\nu_c/\nu_o)4\pi r_c^2(k''(C_{o\infty}k_D/(k_D + k'')). \end{aligned} \tag{4.80}$$

Note that when $k_D \to \infty$ (i.e., the surface reaction is the rate-limiting step), Eq. 4.76 is recovered. When $k'' \to \infty$(i.e., gas-film diffusion is the controlling step), Eq. 4.68 is recovered.

Substitution of Eq. 4.71 into Eq. 4.80 and subsequent integration results in the expression

$$\frac{d_{co} - d_c}{2k''} + \frac{d_{co}^2 - d_c^2}{8D_o} = \frac{\nu_c C_{o\infty}}{\nu_o\rho_c}t. \tag{4.81}$$

The time $(t_b)_{mixed}$ required for complete consumption of the char particle when both diffusion and surface reaction resistances are present is $(t_b)_{mixed} = (\nu_o\rho_c/(\nu_c C_{o\infty}))(d_{co}/2k'') + (\nu_o\rho_c/(\nu_c C_{o\infty}))(d_{co}^2/(8D_o)) = (t_b)_{rxn} + (t_b)_{film}$. Therefore, to account for the simultaneous occurrence of gas–film diffusion and surface reaction is apparent from the above treatment that the combined effect is simply the sum of the two effects because the two processes occur in series.

Shrinking–core model with an ash layer In this model, there are five distinct processes occurring in series: (1) gas–film diffusion of oxidant, (2) oxidant diffusion through the ash layer, (3) surface chemical reaction, (4) diffusion of products through the ash layer, and (5) diffusion of products through the gas- film back to the ambient. As in the case when an ash layer is absent, we assume that processes (4) and (5) do not contribute to the rate–controlling steps, and that the surface chemical reaction rate is of first–order (cf. Eq. 4.74).

Case (1) Rate controlling: gas–film diffusion of oxidant. The rate of oxidant transported through the gas–film is

$$W_o = 4\pi r_{co}^2 k_D (C_{o\infty} - C_{oa}). \tag{4.82}$$

where C_{oa} is the molar concentration of oxidant at the outer surface of the ash layer. Since only gas–film diffusion is rate–limiting, $C_{oa} \approx C_{os} \approx 0$. From considerations related to stoichiometry and mass balance, we have

$$W_c = (\nu_c/\nu_o)W_o = -\rho_c \frac{d}{dt}\left((4/3)\pi r_c^3\right). \tag{4.83}$$

Substituting the expression for W_o into Eq. 4.83, and integrating that Equation, we obtain

$$1 - (\frac{d_c}{d_{co}})^3 = \frac{6k_D C_{o\infty}\nu_c}{\rho_c d_{co}\nu_o} t. \tag{4.84}$$

Therefore, the time $(t_b)_{film}$ for complete consumption of the particle is

$$(t_b)_{film} = \rho_c d_{co}\nu_o/(6k_D C_{o\infty}\nu_c).$$

Case (2) Rate controlling: diffusion through ash layer. Assuming the ash layer to be quasi–steady, the diffusion in the ash layer can be described by a constant effective diffusivity, D_e^*, and the molar flow rate of oxidant through a surface of any radius r in the ash layer can be written in the form $W_o = 4\pi r^2 D_e^* \frac{dC_o}{dr} = \text{constant}$. That W_o is constant is the result of the quasi–steady assumption. Integrating across the ash layer from r_{co} to r_c results in an expression

$$4\pi D_e^*(C_{os} - C_{oa}) = W_o(1/r_{co} - 1/r_c). \tag{4.85}$$

Since surface reaction is infinitely fast and gas–film diffusion resistance is negligible, $C_{os} \approx 0$ and $C_{oa} \approx C_{o\infty}$. Thus Eq. 4.85 can be re–written as

$$W_o = 4\pi D_e^* C_{o\infty}/(1/r_{co} - 1/r_c). \tag{4.86}$$

Substitution of this expression into Eq. 4.83 and subsequent integration results in an expression for the time

$$t = \frac{\rho_c \nu_o d_{co}^2}{24\nu_c D_e^* C_{o\infty}}[1 - 3(\frac{d_c}{d_{co}})^2 + 2(\frac{d_c}{d_{co}})^3]. \tag{4.87}$$

The time $(t_b)_{ash}$ for complete oxidation of the char particle is

$$(t_b)_{ash} = \rho_c \nu_o d_{co}^2/(24\nu_c D_e^* C_{o\infty}).$$

Case (3) Rate controlling: surface chemical reaction. It can be easily shown that this case is equivalent to Case (2) in the shrinking–core model with no ash layer. Therefore, Eqs. 4.77, and 4.78 also apply in this case.

Case (4) Rate controlling: combined effect. Under the quasi–steadiness assumption, the molar flow rate of oxidant through the gas–film is equal to that through the ash layer, which in turn equals the rate of oxidant reacted at the particle surface. Therefore, equating Eqs. 4.75, 4.82 and 4.85, and eliminating C_{oa} and C_{os}, we have $W_o = 4\pi r_{co}^2 K_e C_{o\infty}$, where

$$K_e = \frac{1}{(1/k_D) + (r_{co}/(D_e^* r_c))(r_{co} - r_c) + (r_{co}^2/(r_c^2 k''))}. \tag{4.88}$$

The first, second and third terms in the denominator in Eq. 4.88 respectively represent gas–film diffusion, ash diffusion, and chemical reaction resistance. When gas–film diffusion is rate–limiting (i.e., $D_e^* \to \infty$, and $k'' \to \infty$), Eq. 4.82 (with $C_{oa} \approx 0$) is recovered. When ash diffusion is rate–controlling (i.e., $k_D \to \infty$, and $k'' \to \infty$), Eq. 4.86 is recovered. When surface reaction is rate-determining (i.e., $k_D \to \infty$, and $D_e^* \to \infty$), Eq. 4.75 is recovered. Substituting the expression for W_o, and Eq. 4.88 into $-\rho_c d/dt((4/3)\pi r_c^3) = W_c = (\nu_c/\nu_o)W_o$, and integrating, it can be shown that $(t_b)_{mixed} = (t_b)_{film} + (t_b)_{ash} + (t_b)_{rxn}$. That is, the combined effect is the sum of the individual effects.

4.4.1 Coal–oil/coal–water slurry droplet combustion

The combustion of coal–oil or coal–water slurry droplets constitutes an interesting and complicated process. A model partly, based on recent experimental findings, is formulated in the following. It has been experimentally observed [296, 297] that there are two liquid gasification

regimes, i.e., the slurry droplet surface initially regresses linearly with time, followed by a period during which gasification is characterized by a constant–diameter droplet.

During the regressing–diameter period, water vaporizes from the droplet surface, and agglomeration of dispersed coal particles near the droplet surface occurs due to water depletion at the surface and an increase in particle density. As gasification continues, more and more particles agglomerate at the surface to form a shell, until a critical porosity ϵ_c, is reached. At this point, thickening of the agglomerate layer at the droplet surface occurs until a critical layer of thickness δ_c is formed. The agglomerate thus formed is experimentally determined [297, 298] to consist of a porous shell structure which is saturated with liquid. Transition from the regressing–diameter period to the constant–diameter (also referred to as the rigid–shell period) is thought to occur when both the shell porosity and thickness reach their respective critical values. The rigid–shell period persists until all the water in the droplet is depleted. During this period, the inner surface of the porous shell continues to thicken with a shell porosity ϵ_c. Subsequently, the coal agglomerate is heated, and devolatilized, followed by combustion of the volatiles, and oxidation of the resulting char.

The scenario we consider consists of initially exposing a coal–water slurry droplet with an initial temperature T_o, an initial liquid volume fraction ϵ_o, and diameter of d_{so} to a high ambient temperature T_∞. The total droplet lifetime, t_b is considered to consist of (1) an initial droplet heat–up period $t_{h,1}$, (2) a period $t_{l,1}$ when the droplet surface regresses linearly with time as water vaporizes, (3) a constant–diameter period $t_{l,2}$ during which time a rigid porous shell structure is formed after which all the liquid is completely depleted from the slurry droplet, (4) a period $t_{h,2}$ of heating the rigid shell to a temperature at which devolatilization occurs, (5) a devolatilization period t_{dev}, (6) a volatile combustion period t_{vol}, and, finally, (7) a period t_{char} for char oxidation. An implicit assumption in the model is the absence of micro–explosion or fragmentation of the slurry droplet which may occur under certain experimental conditions [299, 300].

Initial droplet heat-up period During this time, the droplet diameter remains unchanged, and the droplet is being heated from a temperature T_o to T_s, where T_s is the saturation temperature of the liquid in the slurry. At this instant, it is assumed that ignition occurs (i.e., there is no ignition delay period). For mathematical simplicity, and illustration of the treatment, we further assume that radiation from the ambient to the droplet surface is unimportant, and that the Biot number of the slurry droplet is less than 0.1 so that the lumped–capacitance heat transfer

model is applicable. In light of these assumptions.

$$\rho_s(4/3)\pi r_{so}^3 C_{ps}\frac{dT_{cs}}{dt} = 4\pi r_{so}^2 h(T_\infty - T_{cs}), \tag{4.89}$$

where r_s, r_{so}, C_{ps} and T_{cs} are respectively the density, initial radius, heat capacity, and temperature of the slurry droplet. Upon integration of Eq. 4.89, we obtain an expression for the droplet heat-up period, i.e., $t_{h,1} = (\rho_s C_{ps} r_{so}/3h)\ln[(T_\infty - T_o)/(T_\infty - Ts)]$.

Regressing diameter period From experimental data [296, 297], the liquid gasification is determined to be well described by the classical d^2-Law of liquid droplet combustion. Therefore, we write $t_{l,1} = (d_{so}^2 - d_{sc}^2)/K$, K being the evaporization rate constant of the liquid and d_{sc} the diameter of the droplet at the time when the shell attains its critical porosity ϵ_c and thickness δ_c.

Constant-diameter rigid shell period It has been shown [297] that the time required to achieve complete liquid depletion is

$$t_{l.2} = 2\epsilon_o d_{ic}^3/(3Kd_{sc}).$$

where d_{ic} is the initial shell (corresponding to ϵ_c and δ_c) inner diameter. Using a solid mass balance for the shell, d_{ic} and d_{sc} can be obtained from the following relationship, given δ_c and ϵ_c.

$$(d_{so}^3 - d_{ic}^3)(1 - \epsilon_o) = (d_{so}^3 - d_{ic}^3)(1 - \epsilon_c)\ . \tag{4.90}$$

and $d_{ic} = d_{sc} - 2\delta_c$.

Although δ_c and ϵ_c have to be determined empirically, estimates of these quantities can be obtained by assuming the particles to be in contact, and packed as monodisperse spheres with centers arranged in a cubic pattern (i.e., $\epsilon_c = 0.476$), and by inferring δ_c to be equal to a three-particle thickness (from experimental measurements).

Heat-up of the rigid shell period During this period, the shell is assumed to be heated from T_s to a representative devolatilization temperature T_{devol}. The assumption of a T_{devol} is a simplification because devolatilization normally occurs over a range of temperatures. Further assuming the Biot number of the shell is less than 0.1, we obtain

$$\rho_s\frac{4}{3}\pi(r_{sc}^3 - r_{if}^3)C_{ps}\frac{dT_{shell}}{dt} = 4\pi r_{sc}^2 h(T_\infty - T_{shell}). \tag{4.91}$$

where $r_{sc} = (d_{sc}/2)$ and $r_{if} = (d_{if}/2)$. The final (i.e., at the end of the rigid-shell period) inner diameter of the shell, d_{if}, can be calculated [297]

from the expression $(d_{if}/d_{ic})^3 = (\epsilon_o - \epsilon_c)/(1 - \epsilon_c)$. After integrating Eq. 4.91, we obtain

$$t_{h,2} = (\rho_s C_{ps}(r_{sc}^3 - r_{if}^3))/(3hr_{sc}^2)) \ln[(T_\infty - T_s)/(T_\infty - T_{devol})]. \quad (4.92)$$

Devolatilization and volatile combustion period The devolatilization and volatile combustion normally occur relatively fast compared to other processes. For modeling purposes and simplicity, these two time intervals generally may be considered negligible although t_{devol}, in principle, can be estimated once the devolatilization kinetics are known.

Char oxidation period The treatment in Section 4.3 can be used to estimate the char oxidation period.

Total droplet lifetime The total droplet lifetime (t_b) can now be calculated by the relation $t_b = t_{h,1} + t_{l,1} + t_{l,2} + t_{h,2} + t_{char}$.

4.4.2 Pollutant Formation in Coal Combustion

Due to the organic and inorganic constituents of coal particles, typical pollutants formed during the combustion of coal particles include particulate matter, sulfur compounds, nitrogen oxides, carbon dioxide, trace elemental species, trace gases, and polycyclic aromatic hydrocarbons.

The particulate matter is generally divided into two types: smoke and dust or grit. Smoke which comprises soot and droplets of condensed tar is formed as a result of the incomplete combustion of the tar components during the devolatilization of the coal particle. Dust or grit is basically coal ash which originates from the mineral matter in the coal particle. Smaller or finer ash particles are referred to as dust whereas larger or coarses particles are referred to as grit. Dust and grit particles are generally chemically inert and composed largely of stable oxides.

The emission of sulphur compounds (SO_x) during the combustion of coal particles cause not only atmopheric pollution (acid rains) but also corrosion in power plant equipments. Sulphur compounds are formed through a series of reactions involving the organically bound sulphur and sulphur bearing inorganic compounds in the mineral matter (e.g., pyrites) of coal particles. The predominant combustion product is sulphur dioxide (SO_2), with small amounts of sulphur trioxide (SO_3), and a considerable amount of sulphur (approximately about 15%) is retained in the residual coal ash.

Among the nitrogen oxides (commonly referred to as NO_x) generated when coal particles are burnt, nitric oxide (NO) accounts for about 95% (by volume) of NO_x emission with a small fraction (usually less than 5%) of nitrogen dioxide (NO_2). Trace amounts (a few ppm) of nitrous

oxide (N_2O) are also produced. Nitrogen oxides originates from the organic nitrogen present in coal particles and the atmospheric nitrogen. Like SO_x, NO_x emission is responsible for the formation of acid rain. Although the emission of N_2O is relatively insignificant compared to that of NO_x, N_2O plays a role in the greenhouse effect.

In a strict sense, carbon dioxide cannot be regarded as a pollutant because so many life processes depend on it. Carbon dioxide is emitted mainly during devolatilization of coal particles. The concern over the role of carbon dioxide as a pollutant stems from the now well-established observation that the concentration of carbon dioxide in the atmosphere is increasing. An increase in carbon dioxide could cause a significant change in the global climate.

The presence of trace elements in coal particles also cause some environmental concern. Some trace elements are emitted to the atmosphere as vapor during combustion while others remain in the residual coal ash.

In addition to the emission of SO_x, NO_x, and CO_2, emission of trace gases have been reported during combustion of coal particles. Trace gases that have been identified include: methane, ethylene, higher hydrocarbons, carbon monoxide, hydrogen cyanide, hydrogen sulphide, carbonyl sulphide, and carbon sulphide [287].

Volatile species in the form of polycyclic aromatic hydrocarbons (PAH) can be emitted from the coal particles during high temperature (above 450°C) devolatilization [287]. The concern over PAH is their carcinogenicity. The yield of PAH depends strongly on the coal rank; it increases with rank [301].

4.5 Introduction to smoldering combustion

4.5.1 Some characteristics of smoldering combustion

Smoldering can be defined as a slow, low-temperature, and flameless form of combustion [302]. The fire hazards imposed by smoldering combustion are the copious toxic gaseous products from the process and the role of the process in the initiation of unwanted fires by the rapid transition from smoldering to flaming. Examples of smoldering combustion, to name a few, are burning of cigarettes, mattresses, sawdust, paper, cardboards, woodshaving, and fabrics.

Various combinations of physical and chemical factors determine whether a material can undergo self-sustained smoldering. Smoldering can only be self-sustained if the condensed-phase fuel is porous and forms a char. Once smoldering is initiated, the self-sustained mechanism for smolder spread is by means of the heat evolved either from the exothermic oxidative/thermal degradation of the fuel, from the subsequent oxidation of the char, or both. Since the heat source is from the oxidative

processes of the fuel and the char, the importance of oxygen transport and the oxidative reaction kinetics is apparent.

Materials that smolder normally have a large surface to mass ratio, that is needed to provide more reaction sites for oxygen attack. Fuels that are porous or are made of particle aggregates manifest such characteristic. For such fuels, the heat generated from the intrinsic exothermic oxidation reactions will be trapped within the fuel because the internal structures of the fuels form fairly effective thermal insulators. The resulting effect is to slow heat losses, thus sustaining combustion. Since the principle heat source is derived from the oxidative reactions, materials that form chars or degrade exothermically in the presence of oxygen are likely to smolder. The formed chars have a very large surface to mass ratio and a rather high heat of oxidation. The oxidation of char is further facilitated by the catalytic effect of the impurities present in most of the smolder materials.

Since the oxygen transport is, in most case, the controlling mechanism for smolder propagation, the classification of smolder spread can be based on the direction of oxygen transport. In the one-dimensional spread, when the oxygen diffuses in the direction towards the smolder reaction front, the smolder spread is termed *reverse spread*. When the transport of oxygen is in the same direction as the smolder spread, a *forward spread* results. Forward spread rate is found to be slower than the reverse spread. More complete combustion of the fuel is manifested when the fuel material undergoes forward smoldering [302].

4.5.2 Propagation of smoldering

A simple qualitative treatment of smolder spread can be obtained by using the fundamental equation of fire spread [303]. The concept is based on the idea that the spread rate is determined by the rate of heat transfer across the surface of fire inception, which is conceptually defined as the boundary between the burning and nonburning fuel. From conservation of energy,

$$\rho_F V \Delta h = Q''. \tag{4.93}$$

where ρ_F is the density of the fuel (kg/m^3), V the spread rate (m/s), δh (kJ/kg) the enthalpy change (per unit mass) between the fuel at its ignition temperature and the virgin fuel, and Q'' (kW/m^2) is the heat flux across the surface of fire inception. Assuming the diffusion of oxygen and the heat release of the oxidative reactions to be the controlling mechanism of smolder spread, the diffusive mass flux of oxygen (N_o) to the smolder surface can be approximated by

$$N_o \sim D_o(\Delta\rho_o/L) \sim D_o(\rho_{o\infty}/L). \tag{4.94}$$

where D_o is the oxygen diffusivity (m^2/s), $\delta\rho_o = \rho_{o\infty} - \rho_{os}$ is the concentration difference (kg/m^3) between ambient oxygen and oxygen at the smolder surface (assumed to be negligible due to the fast surface oxidative reactions), and L (m), which depends on the size and geometry of the fuel, is a characteristic length for oxygen diffusion. Then Q'' can be expressed as

$$Q'' = (Q_c \rho_{o\infty} D_o / L) - Q_{loss} \tag{4.95}$$

where Q_c (kJ/kg) is the heat released in smoldering combustion per unit mass of oxygen consumed and Q_{loss} is the heat loss flux by radiation and conduction from the smoldering region. If Q_{loss} is too large then smoldering cannot be sustained. If Q_{loss} is not substantial, then from Eq. 4.93 the spread rate is $V \approx (Q_c \rho_{o\infty} D_o / (L \rho_F \Delta h)$.

The above treatment only provides an order of magnitude estimate of smolder propagation because the quantity L cannot be accurately defined. A general model of smoldering propagation has been proposed and discussed by Ohlemiller [304]. Microscopic (on the scale of fuel particle) and macroscopic (on the scale of fuel bed) conservation equations are derived and non-dimensionalized. The resulting model, with fifty-five dimensionless parameters, is too complex to be solvable. However, simplifications (some of them unrealistic) to the model can be made in situations when the limit of small or large asymptotic values for certain dimensionless parameters is realized.